A study of inverted-V auroral acceleration mechanisms using Polar/FAST conjunctions

P. Janhunen[1], A. Olsson[2,1], *et al.*

April 20, 1999

[1] Finnish Meteorological Institute, Geophysical Research, Helsinki, Finland.

[2] Swedish Institute of Space Physics, Uppsala Division, Uppsala, Sweden.

Abstract

We study the inverted-V electron acceleration mechanisms between FAST and Polar altitudes. Nine Polar/FAST magnetic conjunction events were found, out of which five contain inverted-V type precipitation. In the inverted-V events the energy flux at FAST is about 10 times higher than the energy flux at Polar so that an energization mechanism is needed. In cases where the electron distribution at Polar is approximately a single Maxwellian (2 events), a U-shaped potential drop can explain the spectra pretty well. In more complicated multiple-Maxwellian cases (3 events) a U-shaped potential could explain the total energy flux rather well, but not the details of the distribution functions. In the multiple-Maxwellian events, a correlation between a middle-energy electron anisotropy and the occurrence of broadband electrostatic waves at Polar is seen. We suggest that the anisotropy and the waves are causally related and the waves may have a role in electron energization in multiple-Maxwellian events.

1 Introduction

The U-shaped potential drop (Figure 1) is the standard picture of the electric field structure in auroral inverted-V regions, which first appeared in literature almost 30 years ago [*Carlqvist and Boström,* 1970]. The main evidence for such a potential include (1) an inverted-V shape of precipitating electrons showing downward acceleration [*Lin and Hoffman, 1979*] and (2) strong (up to 1 mV/m) perpendicular electric fields detected in the acceleration region and called electrostatic shocks [*Mozer et al.,* 1977]. Also upward accelerated ions are often observed within the acceleration region at 1-2 R_E altitude from the Earth's surface [*Shelley and Collin,* 1991]. Conjugate studies between two satellites [*Reiff et al.,* 1988] also support this picture. Thus one can say that the U-shaped potential picture is able to account for the most important observational findings below about 12000 km altitude on auroral inverted-V precipitation regions.

In this paper we use five auroral conjunction events between Polar (20000-37000 km altitude; only northern hemisphere passees) and FAST (1900-4100 km altitude) to study whether the U-shaped potential can also account for the observations in this altitude range. This is especially interesting since there is new statistical evidence suggesting that a significant stationary potential drop between the ionosphere and Polar altitude is not so common [*Janhunen et al.,* 1999].

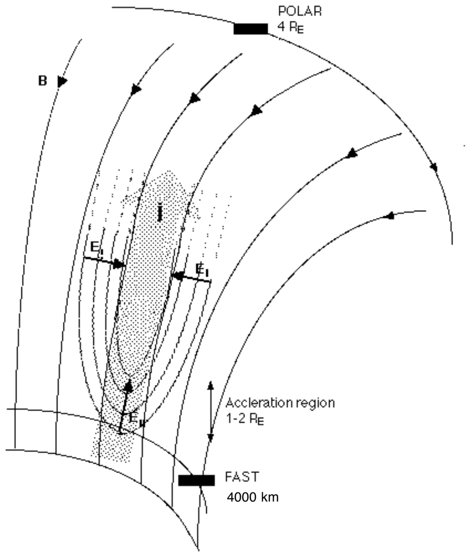

Figure 1: The upward extended U-shaped potential model for auroral electric fields. The acceleration region resides in the $1 - 2R_E$ altitude range. Polar measures the electric field above the acceleration region at about $4R_E$ altitude.

2 Instrumentation

The Polar satellite was launched in February 24 1996 in a polar orbit with 9 R_E apogee and 2 R_E perigee. When Polar crosses the northern auroral oval it is at about 4 R_E altitude. In this study we use Polar data from HYDRA and TIMAS particle detectors, for electrons and ions respectively, as well as the electric field instrument (EFI).

The FAST satellite [*Carlson et al.,* 1998] was launched in August 1996 in a polar orbit with a perigee of 348 km and an apogee of 4159 km. In this paper we use FAST electron data.

For two of the events we use the Canadian CANOPUS ground magnetometer network to assess the temporal stability of the arcs.

2.1 HYDRA

The Polar/HYDRA electron instrument has the energy range of 0.01 - 20 keV. We will use 12 second resolution data which has been integrated in 0-30, 75-105 and 150-180 degree pitch angle bins which will be called parallel, perpendicular and antiparallel, respectively. The raw count rate of HYDRA is proportional to the logarithmic differential energy flux, from which we can compute the particle flux and distribution function by dividing by energy and energy squared, respectively. We will neglect corrections due to the spacecraft potential. These corrections might be needed for energies lower than 30 eV; likewise, at these energies photoelectrons emitted from the satellite, which we also neglect, may also contribute to the measured count rate.

2.2 TIMAS

The Polar/TIMAS (Toroidal Imaging Mass Angle Spectrograph) instrument [*Shelley et al.,* 1995] measures the energy and pitch angle distribution of ions for a wide energy range (15 eV to 32 keV). It can detect four ion species (hydrogen, oxygen and singly and doubly charge helium) and it sweeps through all solid angles in half spacecraft spin of 6 s. In this study we use it mainly to detect the energy and pitch angle characteristics of outflowing ionospheric ions (we concentrate mainly on oxygen). The time of flight of oxygen ions from FAST altitude to Polar altitude is of the order of some minutes, which can be of importance if the arcs are not completely stationary.

2.3 EFI and PWI

Level-0 Polar electric field instrument data [*Harvey et al.,* 1995] is used to estimate the electric amplitude of waves in the 4-10 Hz frequency range. The plasma wave instrument [*Gurnett et al.,* 1995] onboard Polar uses the same antennas as EFI. We use it here to study the correlation between broadband electrostatic wave activity and HYDRA electron anisotropies for frequencies above 28 Hz. Together, EFI and PWI cover the interesting frequency range (except that 10-28 Hz is not covered).

2.4 FAST electrostatic analyzer

The electrostatic analyzers onboard FAST [*Carlson et al.,* 1998] measure the distribution functions of electrons in the range 4 eV to 30 keV. The time resolution varies but is typically about 0.3 seconds which corresponds to about 2 km in ionosphere, which is enough to characterize the precipitation to the accuracy required in a conjugate study between Polar and FAST.

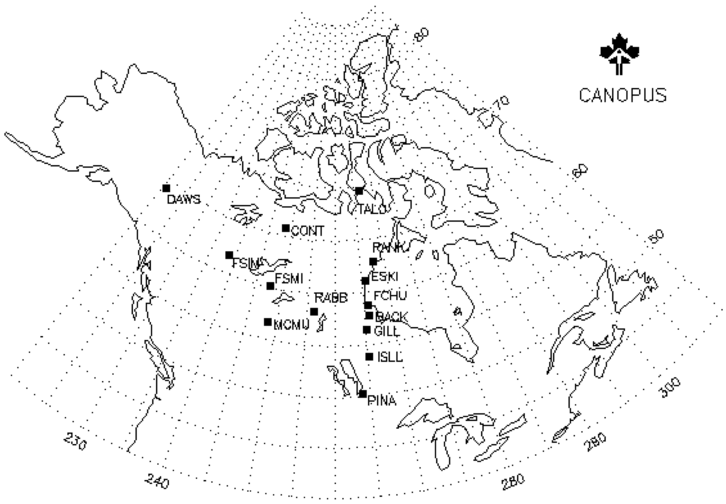

Figure 2: Map of CANOPUS magnetometer sites.

2.5 CANOPUS magnetometer network

CANOPUS is a ground-based magnetometer network covering most of northern Canada (Figure 2). We use it in six cases to put the event in its geophysical context and to evaluate the magnetic disturbance level.

3 Observations

We searched through all events where Polar and FAST are on the same or nearby magnetic field line above the northern auroral zone. We found five events where inverted-V structures were apparent in FAST electron data and four conjunctions which had mainly diffuse precipitation at FAST. We give the times and spacecraft altitudes of the events in Table 1. We also give the smallest equal-time distance of the ionospheric footpoints of the two spacecraft. The smaller this number, the better the conjugacy is.

Date	UT	MLT	FAST alt	Polar alt	Dist	Inv-V	PSI
970603	06:30	19:30	1900	30000	109 km	Yes/MM	On
970606	05:31	20:00	2200	26000	9 km	Yes/MM	On
970608	10:43	18:30	2100	26000	7 km	Yes/MM	On
970615	02:35	20:30	3100	20000	388 km	Yes/SM	Off
970629	01:35	18:40	3600	27000	145 km	Yes/SM	Off
970710	21:39	18:30	4100	24000	188 km	No	Off
970720	16:22	05:20	3200	29000	62 km	No	Off
980727	06:40	06:40	2800	35000	54 km	No	On
980811	02:58	04:15	3400	37000	163 km	No	Off

Table 1: The FAST/Polar auroral conjunctions. Each FAST auroral traversal lasts about 2 minutes; the universal and mean local times given are approximately at the center of each event, or when the most important arcs were seen. The minimum equal-time distance of the footpoints in the ionosphere is also given. In five events, inverted-V arcs were seen. In 970615 and 970629, HYDRA electron spectra is of single-Maxwellian (SM) rather than multiple-Maxwellian (MM) type most of the time. The Plasma Source Instrument (PSI) [*Moore et al.*, 1995] onboard Polar is operating in four events, so that low-energy particle, electric field and wave measurements may be affected and have to be interpreted with care. The last four events were diffuse precipitation events.

For magnetic field line mapping between Polar and FAST we employ the Tsyganenko-95 (T95) model with true dipole tilt, $K_p = 3$, Dst= 0 and 2 nPa solar wind dynamic pressure for the external part and the IGRF model for the internal part. Varying the K_p index or the models produced only small differences in the ionospheric footpoints.

We also tried to estimate the possible mapping error by another method, which is to take the observed maximum magnetic field during the event at Polar and subtract a model magnetic field from it, to obtain a variation field. Assuming that the variation field is caused by field-aligned current, the magnitude of the variation field scales as $\sqrt{B}$ between Polar and the ionosphere. Although we know the direction of the variation vector at Polar, it is difficult to know the direction below the spacecraft. Consequently we computed the mapping error for different directions. Selecting the worst case shows that a mapping error as large as 10 degrees in longitude can be produced by this estimation. In latitude the error is much less. A longitudinal error in mapping does not matter if the arcs are east-west aligned.

We will use three categories for the events: diffuse Maxwellian events (diffuse precipitation at FAST, approximately Maxwellian spectra at HYDRA), single-Maxwellian events (inverted-V precipitation at FAST, HYDRA spectra most of the time approximately Maxwellian) and multiple-Maxwellian events (inverted-V precipitation at FAST and HYDRA spectra most of the time composed of more than one Maxwellian). Those events that we call "single-Maxwellian" here are usually not really that in the mathematical sense, because it is very rare to find a purely single-Maxwellian spectrum in observational data. If a spectrum has only a single peak and is not "box-like" (does not have a wide plateau), it is termed single-Maxwellian, otherwise multiple-Maxwellian in this paper.

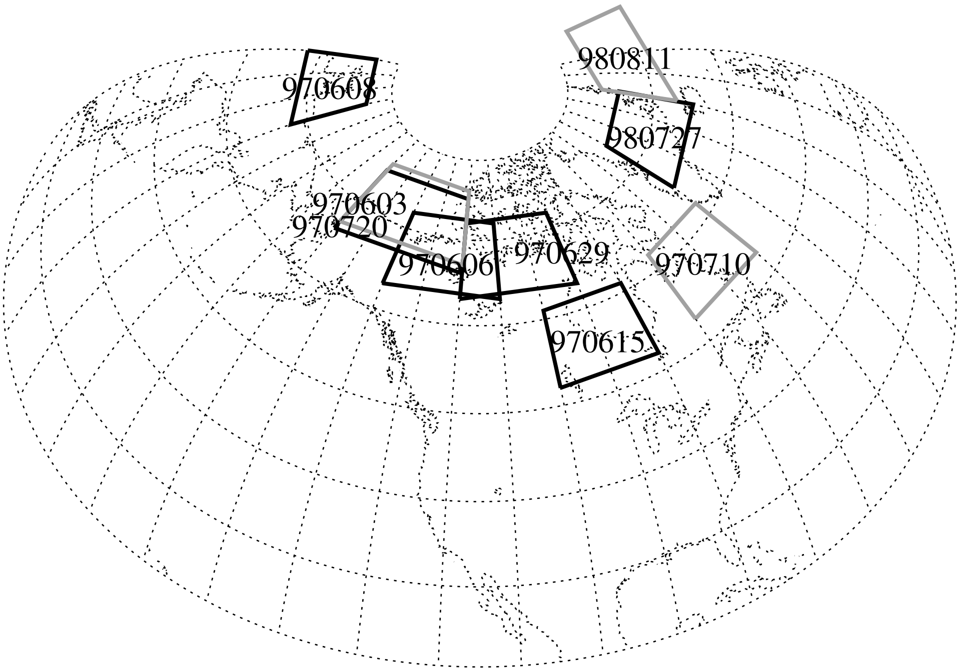

Figure 3: Summary plot of all nine events. The black boxes are shown in more detail in Figure 4 below while the gray ones are not. All the gray boxes are diffuse events.

In Figures 3 and 4 we show the location of the events on the world map and the FAST/Polar mapping for six of the events. The maps are not shown for three diffuse events (980727, 970720, 980811), these events are not discussed in much detail below. In Table 1 we gave the smallest equal-time distance of the ionospheric footpoints, which is one measure of the goodness of the conjugacy. However, when evaluating the events one must also take into account where the arcs are. Thus, for more accurate characterization, Figure 4 must be studied to see where the spacecraft are with respect to the arcs at each moment of time.

3.1 Diffuse precipitation events

In four events (Table 1) the electron precipitation at FAST was mostly of the diffuse type and seemingly coming from a Maxwellian source plasma.

In Figure 5 we show HYDRA and FAST energy fluxes for 970710. After Polar and FAST have been mapped to a common geographic latitude (ionospheric footpoint), they have a time difference which has been indicated by colorful dots in the upper panel (see the figure caption for explanation of the coding). The time difference can also be inferred from the numeric time labels given in the two upper panels. The integrated energy fluxes (Figure 5, third panel) match pretty well (disregarding the energy flux peak in FAST at about 64 GLAT which is probably a temporal variation). This serves as a first consistency check for the correctness of the mapping, and also shows that in the absence of inverted-V type precipitation, the measured energy fluxes by high and low altitude spacecraft are comparable. In the other diffuse events (970720, 980727, 980811) we can also confirm these findings.

FAST energy fluxes tend to be on the average somewhat higher (factor of roughly

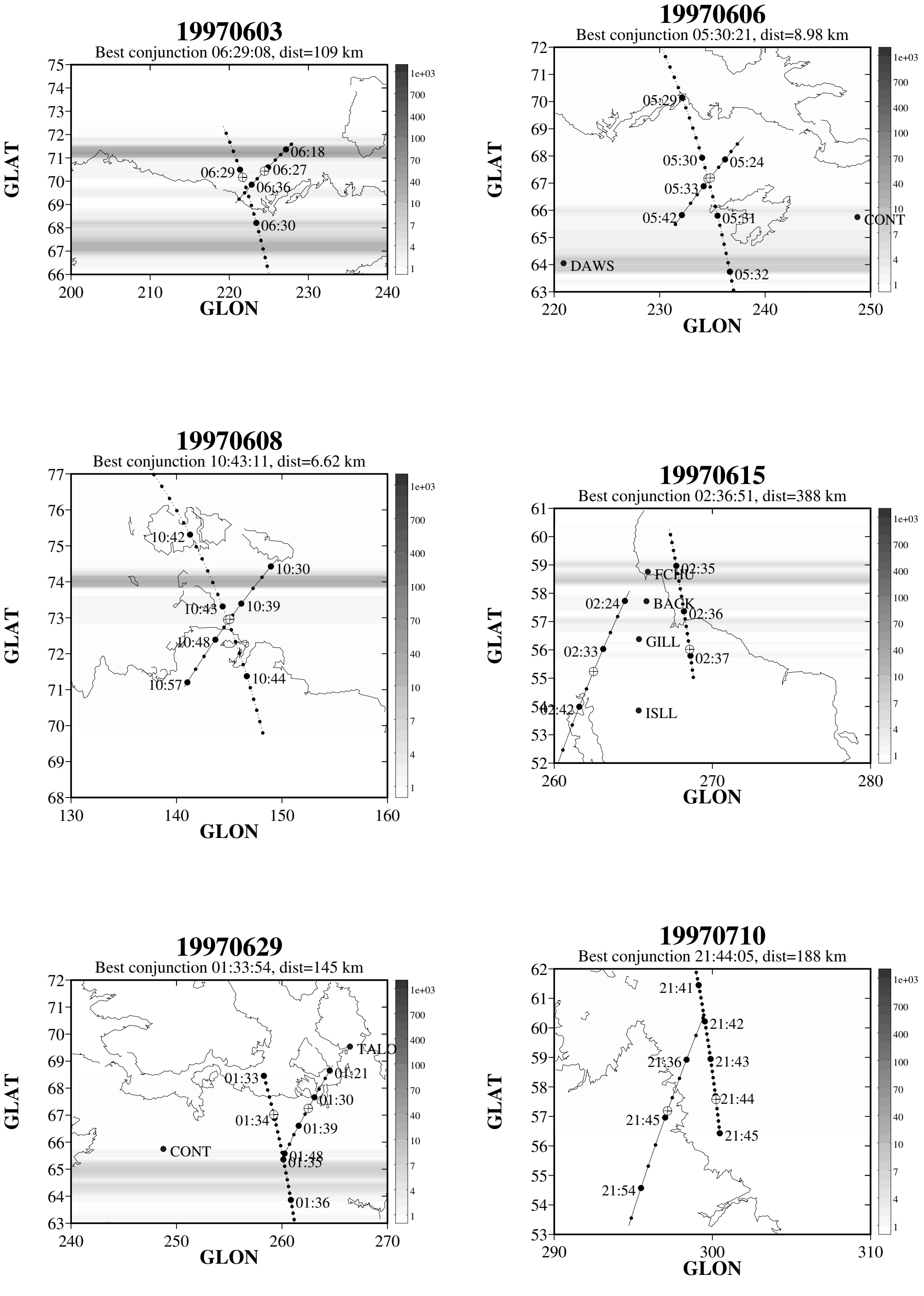

Figure 4: Event maps for all inverted-V events and one diffuse event (970710). The equal-time minimum position of Polar (solid) and FAST (dotted) is shown with open circles. The energy flux of FAST in units of erg cm^{-2} s^{-1} has been indicated by shading by assuming uniformity in the east-west direction.

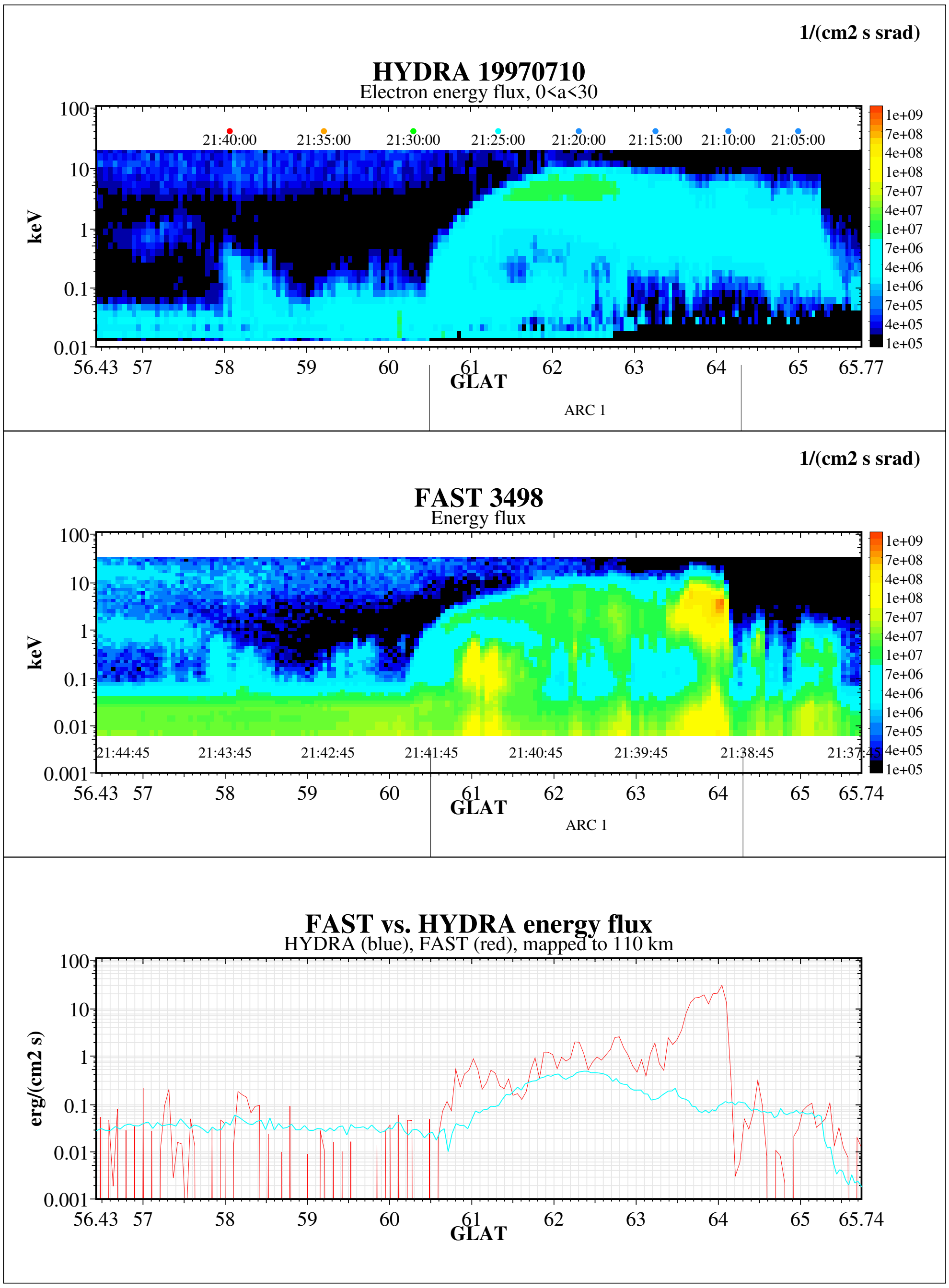

Figure 5: HYDRA/FAST energy fluxes for 970710, which is a diffuse auroral event containing no inverted-V type precipitation. The upper panel shows HYDRA electron energy flux in the parallel direction (averaraged from 0 to 30 ^{o} pitch angle). The time difference between HYDRA and FAST is indicated by red, orange, green, blue and dark blue dots corresponding to <5, 5-10, 10-15, 15-20 and >20 min time differences, respectively. The middle panel shows the corresponding quantity for FAST, mapped to the same geographic latitude. The arc is marked in the two upper panels. The third panel shows the integrated energy flux for both satellites when both quantities are mapped to the ionosphere. Despite some temporal difference, similar features can be recognized in FAST and HYDRA energy fluxes. FAST energy fluxes are about 2-3 times higher than HYDRA fluxes on the average in diffuse events.

2 to 3) than HYDRA fluxes in all four diffuse events. However, the difference is clearly less than for inverted-V events which are discussed next.

3.2 Single-Maxwellian inverted-V events (970615, 970629)

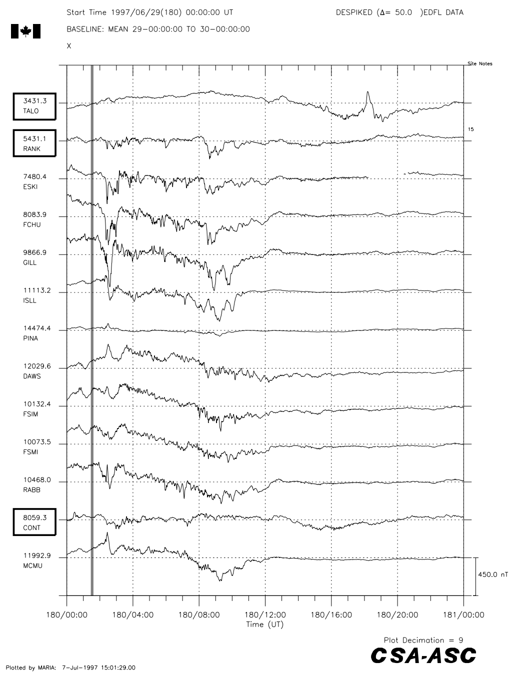

Figure 6: CANOPUS data for 970629. The event time is marked with a gray vertical line. Stations closest to the event are framed. See Figure 2 for the map of all CANOPUS stations.

In Figure 6 we show CANOPUS data for 970629. In this event, both FAST and Polar propagate southward and the three most nearby CANOPUS magnetometers (TALO, RANK, CONT) show only small variations during the interesting time, which is about 01:35 and is marked with gray line in Figure 6.

Event 970615 takes place in northern Canada as well, and CANOPUS variations are likewise small (data not shown).

In Figure 7 we show the HYDRA/FAST energy fluxes mapped along the magnetic field to geographic latitude of the ionosphere for 970615. We identify three auroral arcs in FAST data which are marked in the figure. Notice that the time increases in the direction where the geographic latitude decreases because the satellites are moving southward. The matching of precipitation features is improved if we shift FAST latitude by 0.6 degrees; this shift is done in all our data processing concerning event 970615, but not when data are plotted. The integrated energy flux in FAST is clearly larger (at least one order of magnitude) than in HYDRA during the arcs. During the time when the energy flux discrepancy is largest (arc 1) the temporal difference between HYDRA and FAST is more than 15 minutes. During arc 2 and arc 3 the temporal difference is smaller, 5-10 minutes, and the energy flux discrepancy is roughly 10.

In event 970629 (data not shown) the energy flux discrepancy is even larger (a factor of about 100), but the temporal difference is also rather large (15-25 minutes).

Figure 8 shows TIMAS ion data for 970615. During arcs 2 and 3 the upgoing oxygen energies are small (less than about 200 eV). There are some oxygen ions

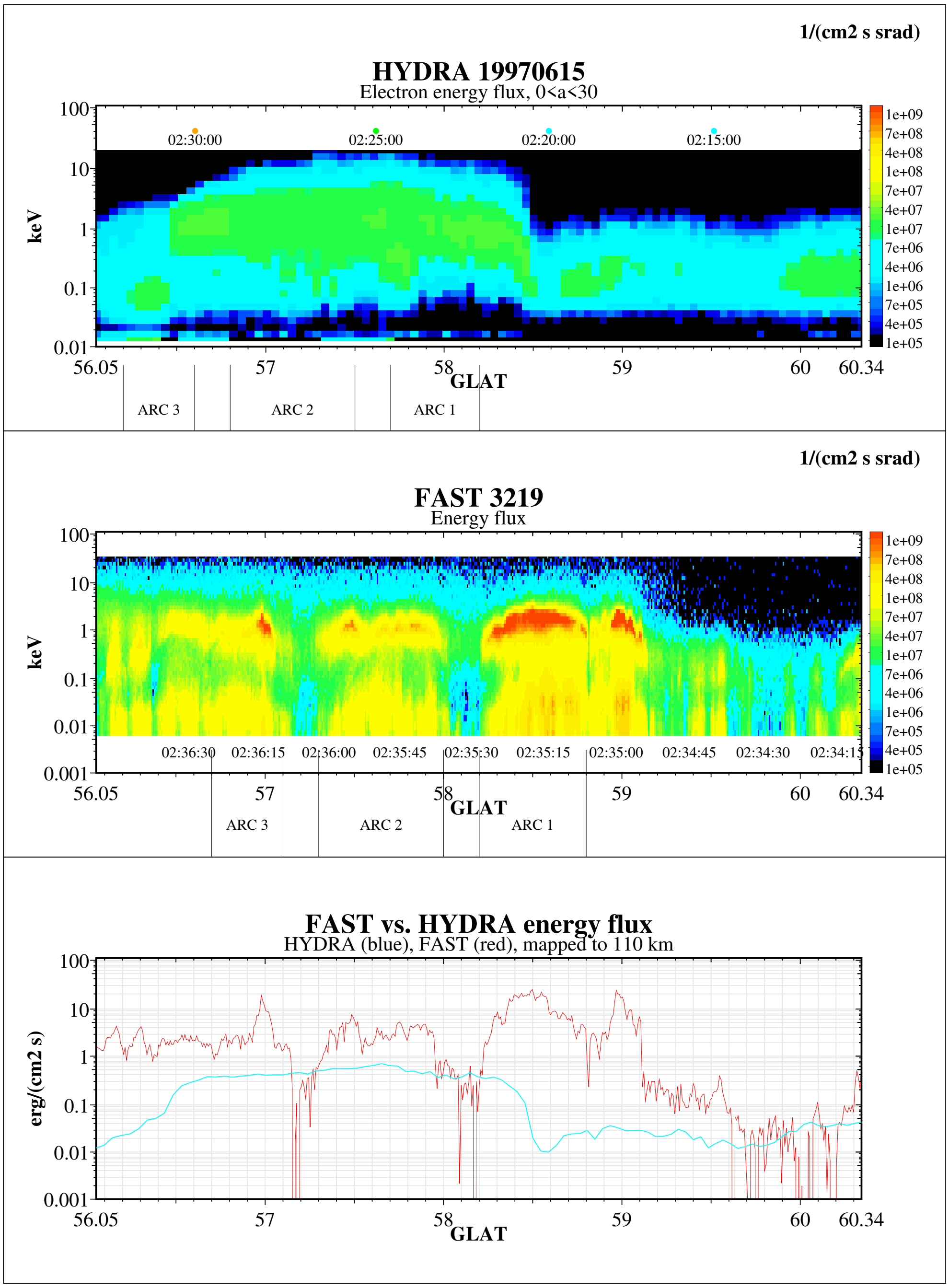

Figure 7: HYDRA/FAST energy fluxes for 970615, which is a single-Maxwellian inverted-V event. The panels correspond to those shown and explained in Figure 5. Here, the FAST energy flux is clearly larger than HYDRA during discrete arcs. In further data processing of this event we have shifted FAST data by 0.6 degrees; it can be seen that this improves the matching of the panels. The shift means that the arc orientation probably differs somewhat from east-west orientation in this event.

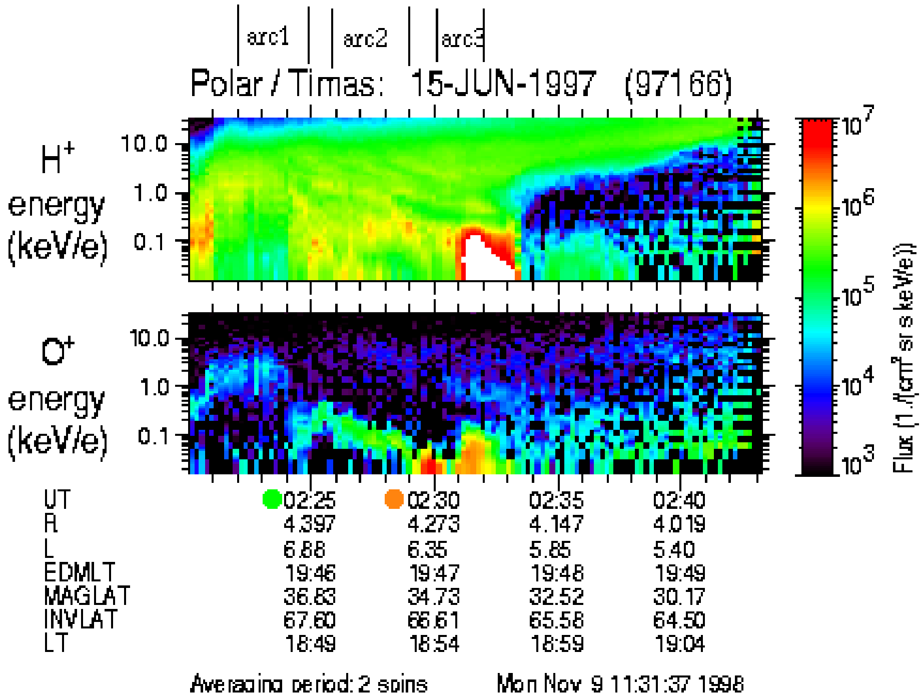

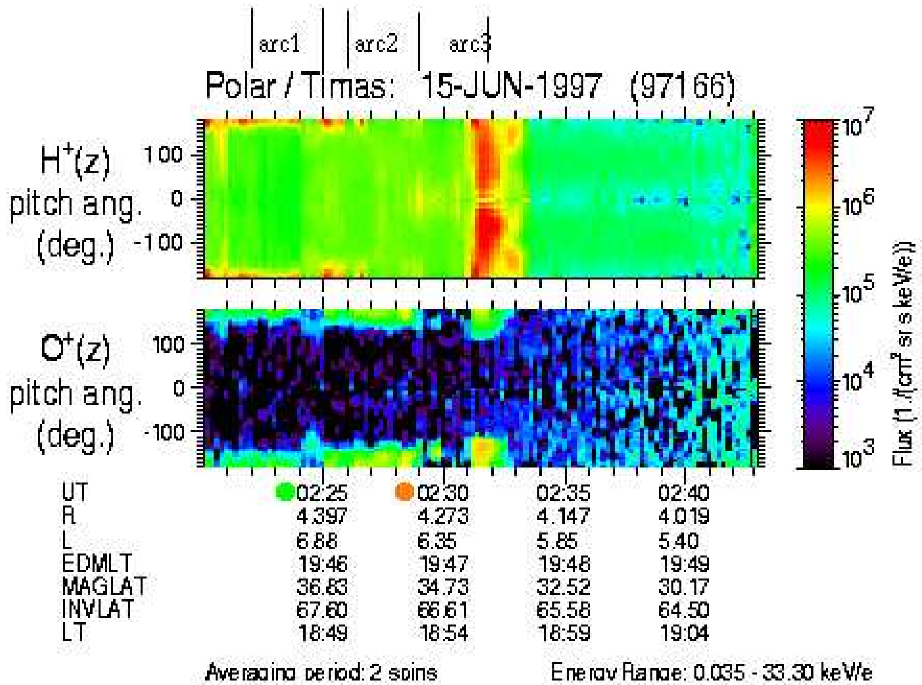

Figure 8: TIMAS ion data for 970615. Upper panel displays the particle fluxes as a function of time and energy, and lowert panel as function of time and pitch angle.

at higher energies also, but they have a rather isotropic pitch angle distribution (this cannot be deduced from the figure but we verified it using the data files). At arc 1 the upgoing oxygen has a higher energy, about 1-2 keV. Thus, arc 1 is compatible with a potential drop estimated from the FAST peak, but arcs 2 and 3 are not. The time difference is the largest at arc 1 (and the sign is such that HYDRA measures the region before FAST so that the oxygen time of flight effect does not help to reduce the time difference) and becomes better at arcs 2 and 3, so as a whole 970615 ion data do not show clear evidence for energization of the oxygen by a potential drop.

For 970629 (data not shown), TIMAS data show that there is outflowing oxygen whose energy (again up to 2 keV) is qualitatively in agreement with FAST peak energy. Thus the oxygen ions in this event are compatible with a potential drop with magnitude of 1-2 kV.

3.3 Multiple-Maxwellian inverted-V events (970603, 970606, 970608)

Event 970603 takes place over the northern coastline of Alaska and Canada, and from CANOPUS data (not shown) we see that there is a substorm going on close to FCHU. The nearest CANOPUS stations DAWS and CONT show about 200 nT variations, and our event occurs northward of these, so it is likely that the disturbance at the event is less than this. Event 970606 is also located in the arctic Canada, and the conditions are quiet according to CANOPUS (data not shown). The temporal mapping between Polar and FAST is close to optimal for 970603. By optimal mapping we mean that zero temporal difference occurs at some of the arcs. The temporal mapping in event 970606 is not quite optimal (time difference is more than 9 min). Event 970608 happens over northeastern Siberia so CANOPUS data cannot be used. This event has good mapping (2-10 minutes time difference during the arcs; concerning the time differences, see the colorful dots in the panels).

In Figures 9 and 10 we show HYDRA and FAST energy fluxes for 970603 and 970606, respectively. In all cases, the energy flux at FAST is the same or larger (sometimes much larger) than at Polar. During the discrete arcs when inverted-V precipitation can be seen, FAST energy flux is typically about 10 times higher than HYDRA energy flux.

By computing the ratio of the distribution function in the parallel and perpendicular directions we can get an estimate of the anisotropy of the distribution. In Figures 11 and 12 we show this anisotropy for 970603 and 970606, respectively, together with wave amplitudes summed from the PWI and EFI instruments (which use the same antenna booms) over two frequency bands, 4-10 Hz (EFI) and 28-1000 Hz (PWI). From the quick-look spectrograms of PWI (not shown here) we see that the most important electrostatic wave activity is below 1 kHz. The frequency band 10-28 Hz would also be interesting but is not measured by either of the instruments. In all our multiple-Maxwellian events, the plasma source instrument (PSI) onboard Polar is on. The PSI operation does create spurious waves in the surroundings of the spacecraft, and one must be very cautious to interpret wave data. However, we see no reason how PSI could cause the correlation between the electrostatic wave bursts and anisotropy occurrences. Furthermore, correlated anisotropies and wave bursts are also occassionally seen in our non-PSI events.

In 970603, during arc 2 (Figure 11), HYDRA data show clearly superposed Maxwellians during the whole inverted-V arc. Almost all the time there is $f_{\|} > f_{\perp}$ anisotropy and wave activity. During arc 1 we have superposed Maxwellians as well, and we see that when the anisotropy moves to somewhat higher energy (up to a few hundred eV), the wave activity also intensifies and seems to move to somewhat higher frequency (PWI vs. EFI intensity relatively increases). The largest anisotropy occurs at GLAT=69, which is a clearly identifiable peak in PWI wave data. A similar correlation between anisotropy and waves occurs also in the other multiple-Maxwellian event, 970606 (data not shown).

Figure 13 shows TIMAS ion data for 970606. During the arcs the energy of the outflowing oxygen is small (<200), except for one brief appearance at about 1-2 keV at 05:45 UT, but the pitch angle of these higher energy oxygen ions is roughly perpendicular (this cannot be seen from the figure, but we checked it from the data files where the fluxes are stored as functions of both pitch angle and energy). The time difference is favourable for detecting ions because HYDRA measures the region a few minutes after FAST for arc 1 (for arc 2 the time difference is larger than 10 minutes). From the FAST peak one would have expected to find 1-2 keV upgoing oxygen with most parallel energy, if the FAST peak is produced by a potential drop.

In event 970603 (TIMAS data not shown) there is a low-energy (<200 eV) upgoing oxygen population during arc 2, and simultaneously a higher energy one

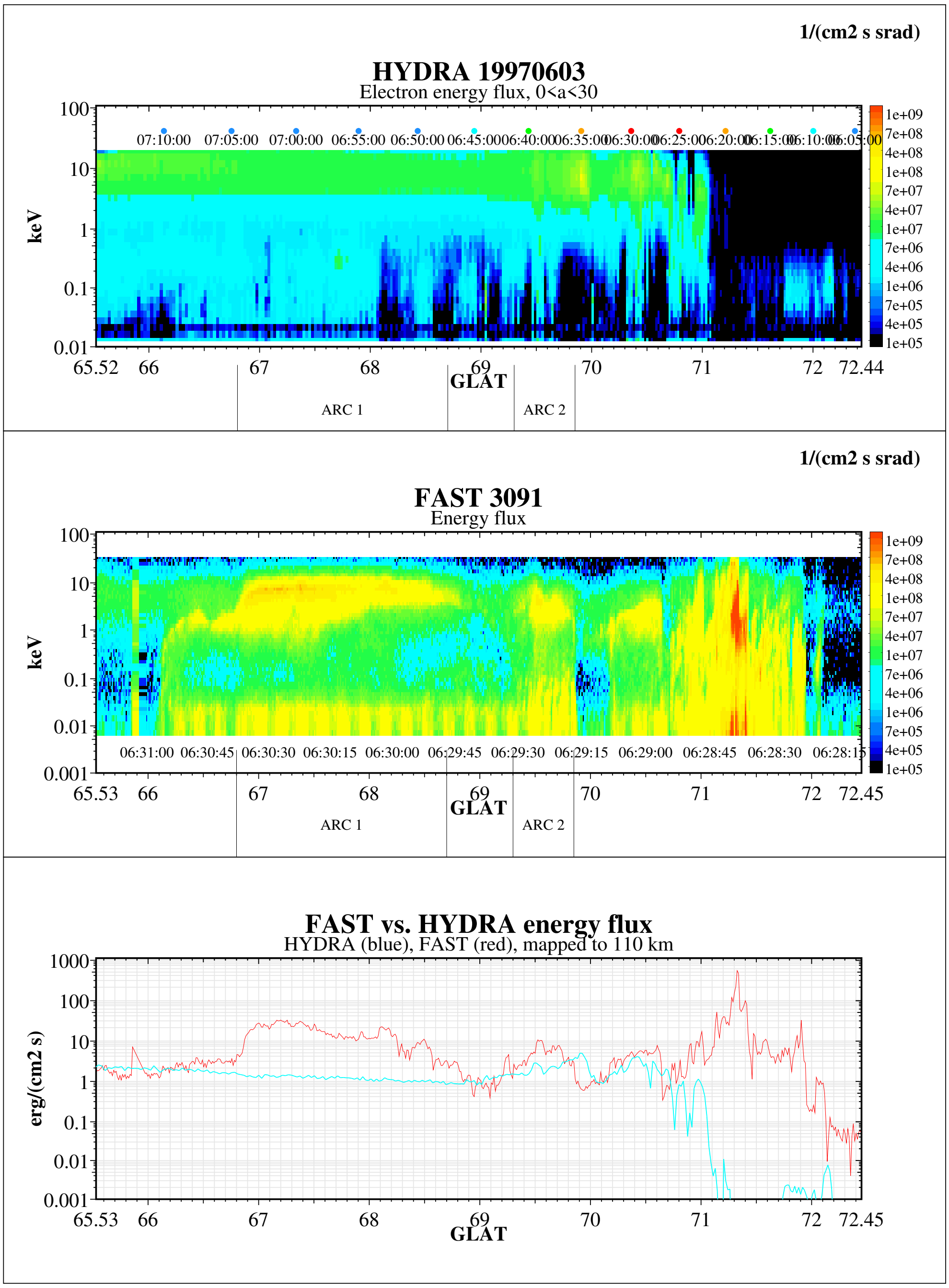

Figure 9: HYDRA/FAST energy flux for 970603 (same as Figure 7). When inverted-V precipitation is seen, FAST energy flux is about 10 times higher than HYDRA.

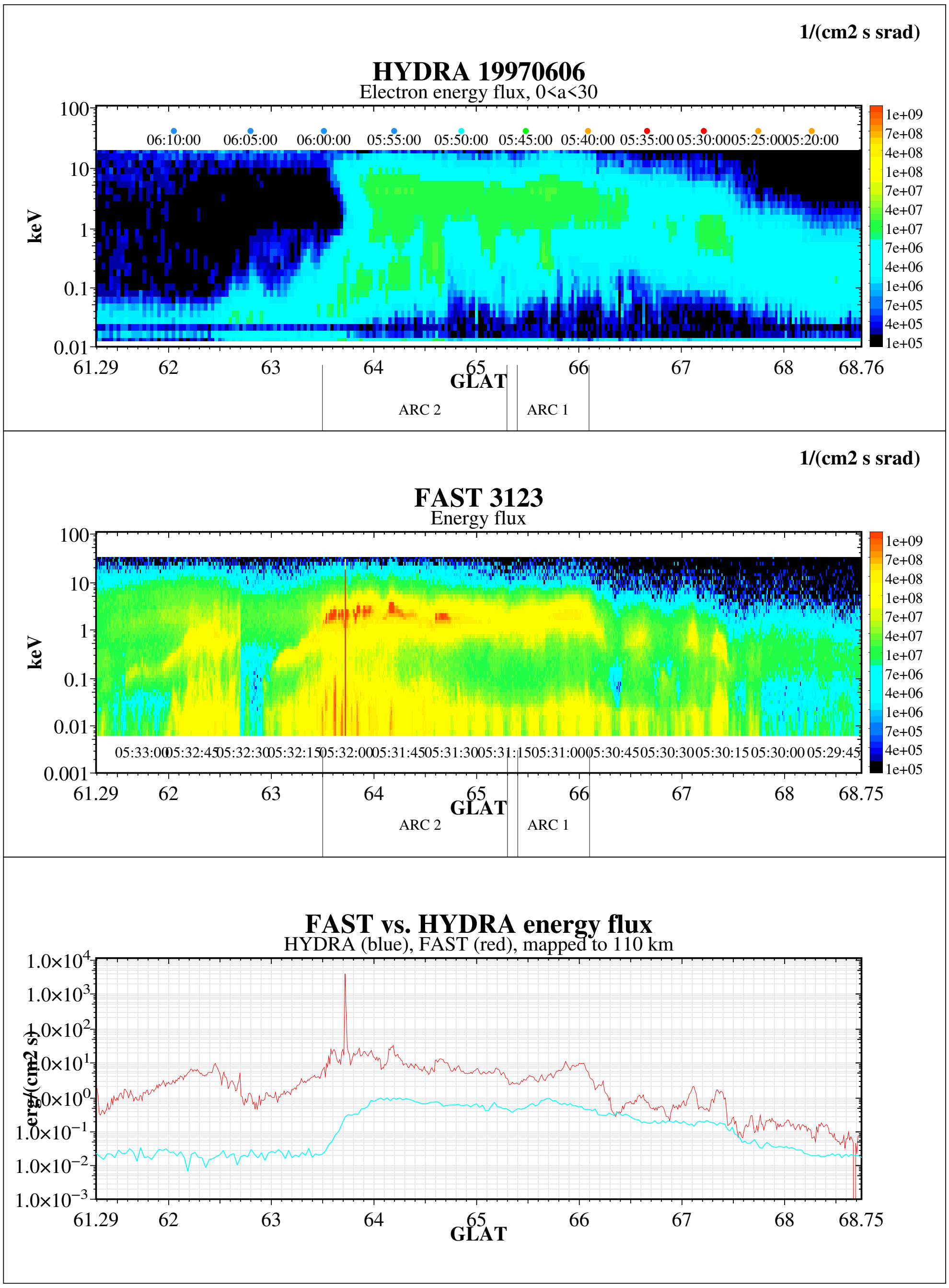

Figure 10: HYDRA/FAST energy flux for 970606 (same as Figure 7).

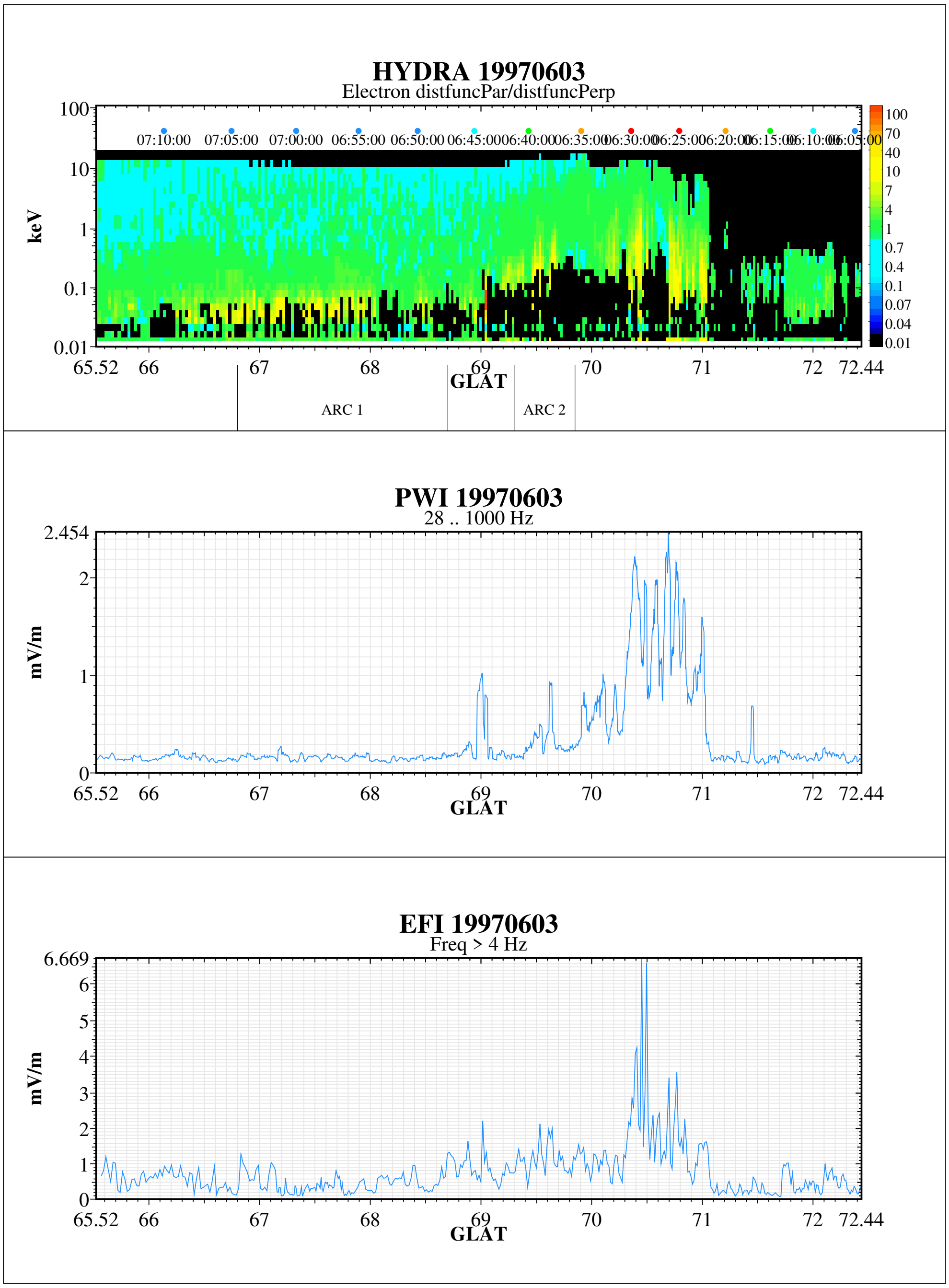

Figure 11: Upper panel: HYDRA parallel vs. perpendicular anisotropy ($f_{\|}/f_{\perp}$). Middle panel: PWI electric wave activity between 28 Hz (the lower threshold of the instrument) and 1 kHz (a limit above which the broadband activity starts to fade and other wave phenomena might interfere). Lower panel: EFI instantaneous electric field amplitude in the 4-10 Hz frequency range. $f_{\|} > f_{\perp}$ anisotropies are seen to be correlated with waves, for example, at 69 GLAT. The PSI instrument is on in this event, so PWI and EFI data must be used very cautiously. There is no reason why the correlation could be caused by PSI, however.

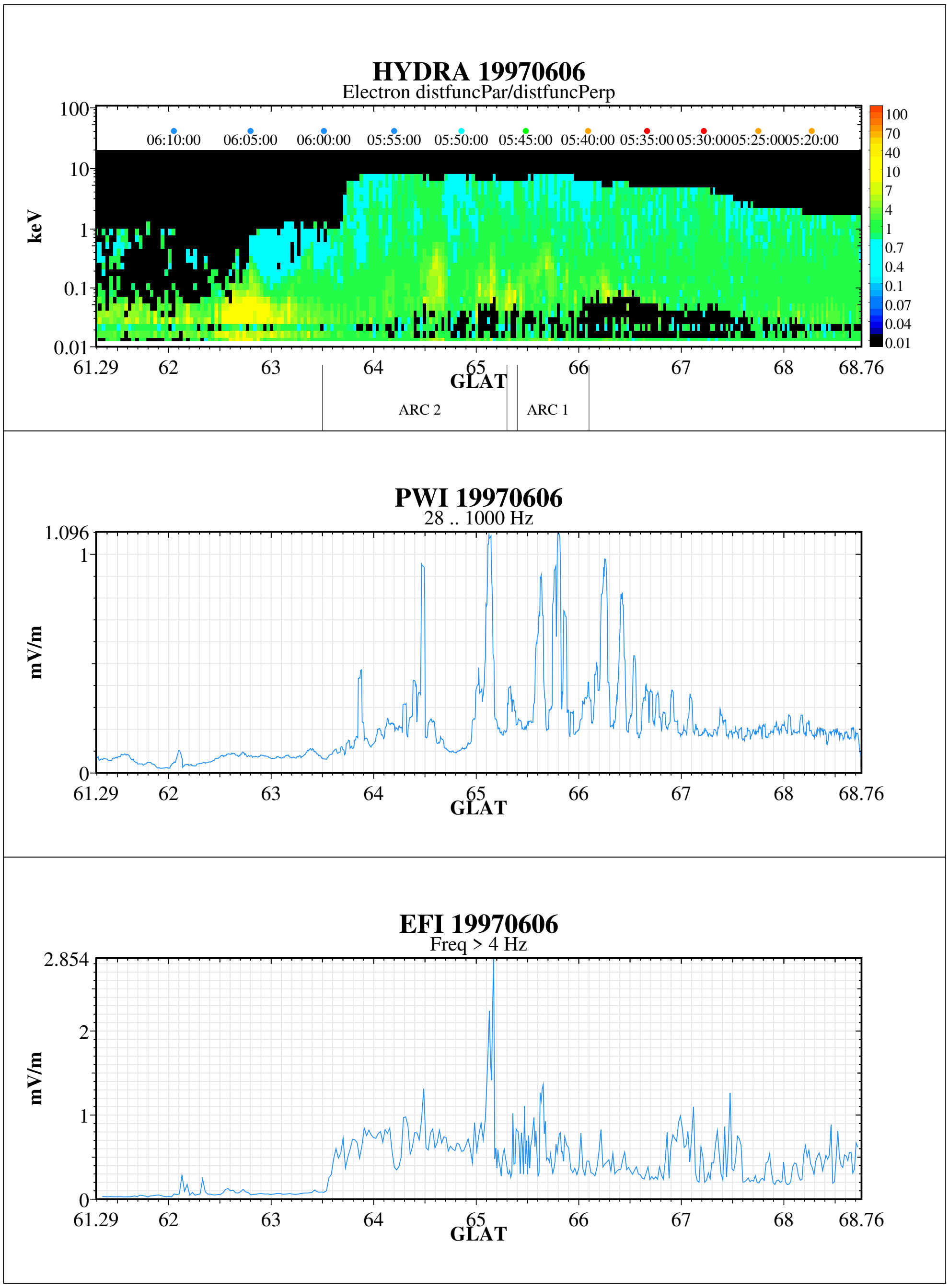

Figure 12: Anisotropy and wave amplitudes for 970606 (same as Figure 11). Also here the $f_{\|} > f_{\perp}$ anisotropies (yellow and red) are correlated with waves. PSI is on in this event as well.

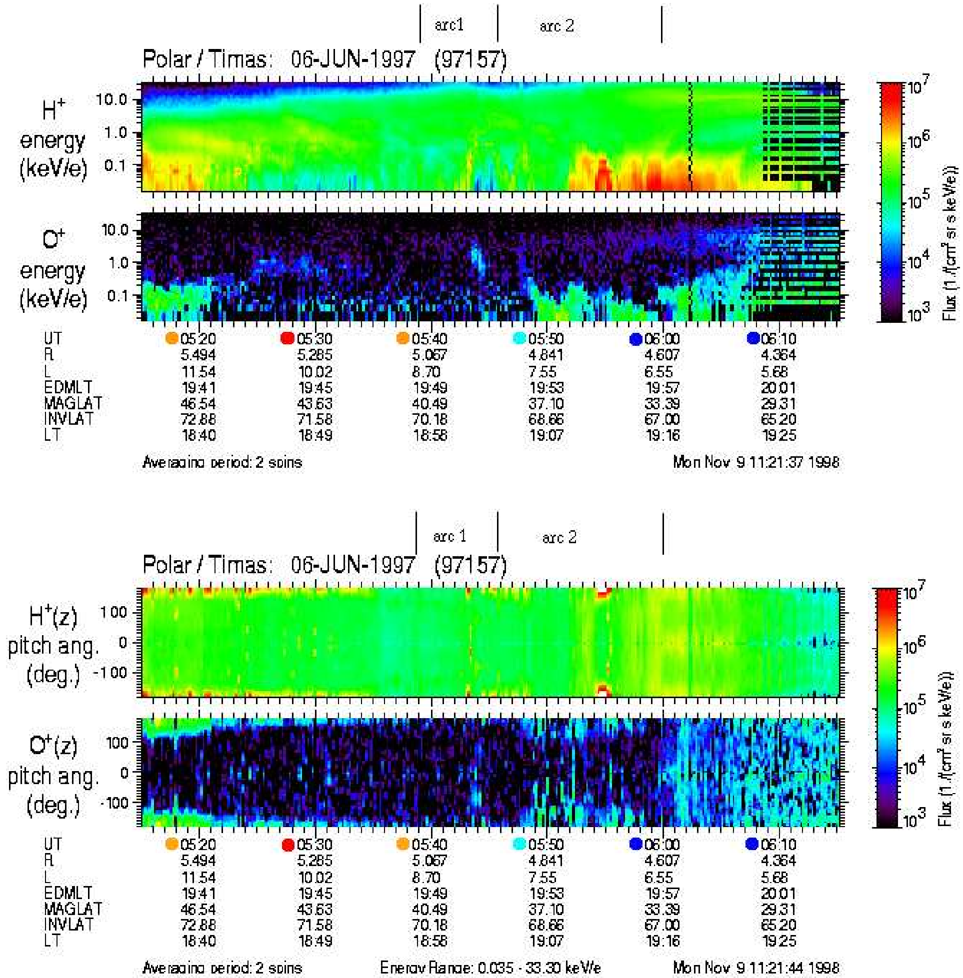

Figure 13: TIMAS ion data for 970606 (same as Figure 8).

(around 2-5 keV) whose intensity is anyway smaller. The higher energy population is extended over all pitch angles (this was again checked from the data files), however, and therefore does not represent an upgoing beam. The existence of two upgoing oxygen populations at different energies does not really speak in favour of a static potential drop of either magnitude (the magnitude would not correspond to the peak energy in FAST anyway, which is 5-8 kV) but probably indicates the existence of temporal variations and/or inductive-type downward parallel electric fields which accelete oxygen ions sporadically and locally. During arc 1 there is an upgoing oxygen population at 1 keV. The FAST peak is at 3 kV in this case.

In event 970608 (data not shown) only low energy oxygen is seen. In this event the time difference is small. So the oxygen data do not support the existence of a U-shaped potential drop in 970608.

4 Discussion and conclusions

By scanning through all thus far available data, we have found nine Polar/FAST auroral conjunction events. Four of the events show only diffuse precipitation. We are especially interested in the five events which have inverted-V type precipitation to be able to study possible acceleration mechanisms between Polar and FAST altitudes. Of the five inverted-V events, two were classified as single-Maxwellian events and the remaining three multiple-Maxwellian events, according to the dominant type of HYDRA electron distributions observed. The term "single-Maxwellian" must not be taken literally, but any spectrum which has only a single peak and does not have a wide plateau is termed "single-Maxwellian" in this paper. If broken down into Maxwellian components in the mathematical sense, such a spectrum may well contain more than one component.

4.1 Single-Maxwellian events

In Figure 14 we show 8 examples of HYDRA spectra taken during inverted-V precipitation of 970615. We have accelerated HYDRA data through a potential drop [*Evans,* 1974] that was determined from the corresponding FAST data by finding the peak position. A latitudinal shift of 0.6 degree is included in this event. The unaccelerated spectra are also shown as the left member of each plot pair for comparison. The HYDRA spectra have a single-Maxwellian character (possibly accelerated by a few tens of eV), while FAST spectra during the discrete arcs show an inverted-V type signature where the peak is around 1 keV. The accelerated HYDRA spectra match with FAST spectra pretty well in this case.

For the other single-Maxwellian event 970629 (Figure 15) the HYDRA electrons are colder and do not produce an equally good match after accelerating them by the FAST peak potential. The HYDRA spectra are deformed a bit from a Maxwellian shape, which adds to narrowness of the spectra after acceleration so that they fail to reproduce measured FAST spectra to some extent. If the energization is due to a potential drop in 970629, some nonadiabatic process has to smear the spectra before the particles reach FAST altitude.

In Figure 16 we show the accelerated HYDRA energy flux for 970615 for all data points as a spectrogram plot. Comparison with the unaccelerated version (Figure 16, lower panel, dotted blue line) shows that letting HYDRA data go through a potential drop causes energization which improves the correspondence with FAST energy flux, which is not unexpected. Notice that the shift of 0.6 degrees should be done in the lower panel of Figure 16.

For 970629 (Figure 17) the match after acceleration is not as good as for 970615, as noted above. The coldness of the HYDRA population and its slightly deformation from a Maxwellian character makes the energy flux after acceleration too small in this case.

4.2 Multiple-Maxwellian events

In Figures 18 and 19 we show the effect of potential drop acceleration on HYDRA data in a multiple-Maxwellian event. The line spectra (Figure 18) show that the matching of HYDRA and FAST spectra cannot be very good because HYDRA data consists of two or more peaks, while FAST has only a single peak. The small energy peak of HYDRA, after accelerated by a potential drop, becomes a peak in the correct location (because the accelerating potential was taken from FAST), but it is too narrow and too high. Likewise, the higher energy peak of HYDRA becomes a smaller peak at somewhat higher energy, which is absent in the FAST data. In other words, the integrated energy fluxes (Figure 19, lower panel) match

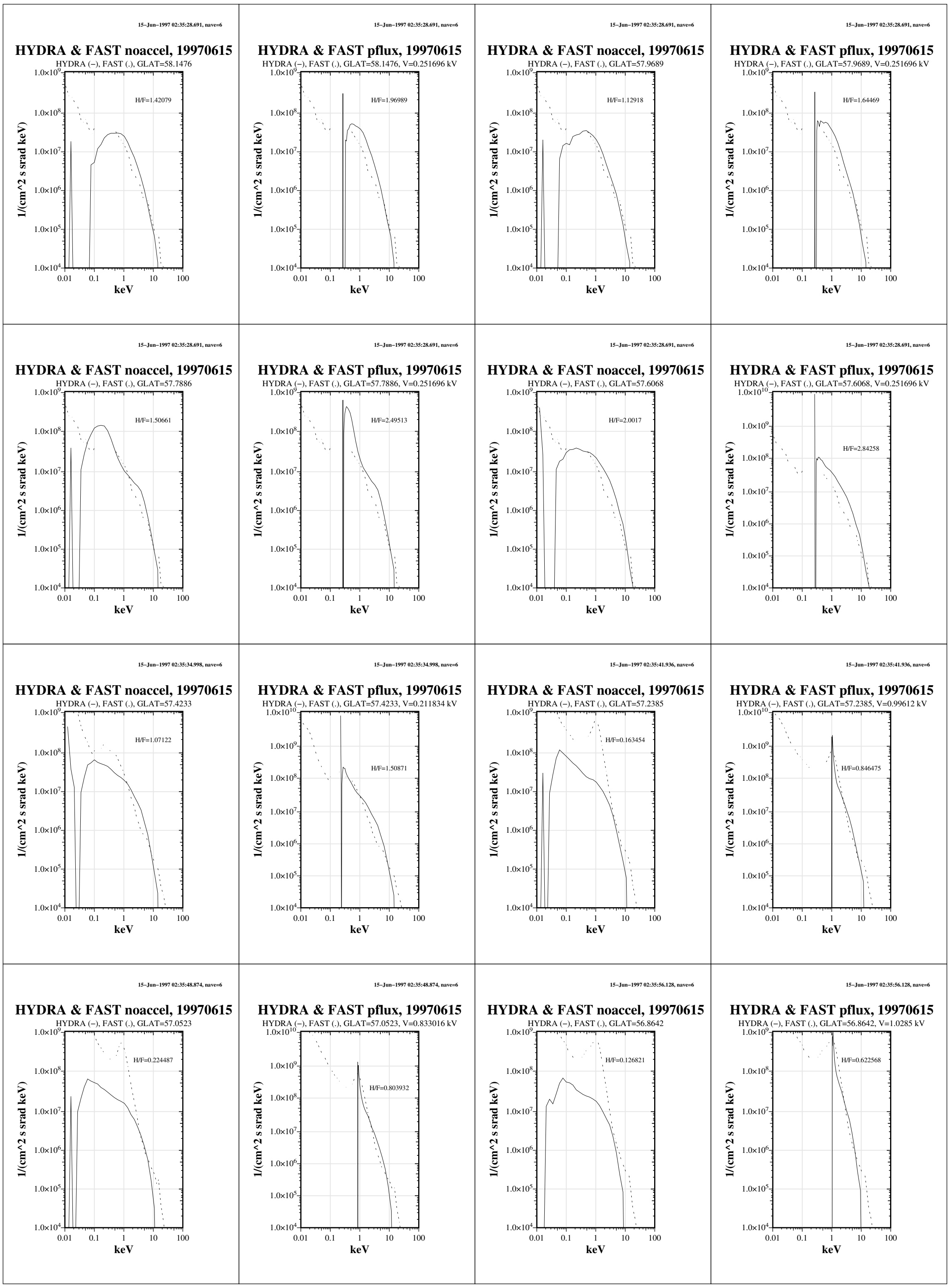

Figure 14: HYDRA (solid) and FAST (dotted) particle fluxes for 970615 (a single-Maxwellian event). The plot contains 8 pairs of nonaccelerated/accelerated line spectra, selected uniformly during inverted-V precipitation. The accelerating voltage has been found from the peak position of FAST (with 0.6 degree latitudinal shift). We see that the nonaccelerated HYDRA spectra are mostly single-Maxwellian. After acceleration, the correspondence with FAST is good in this event.

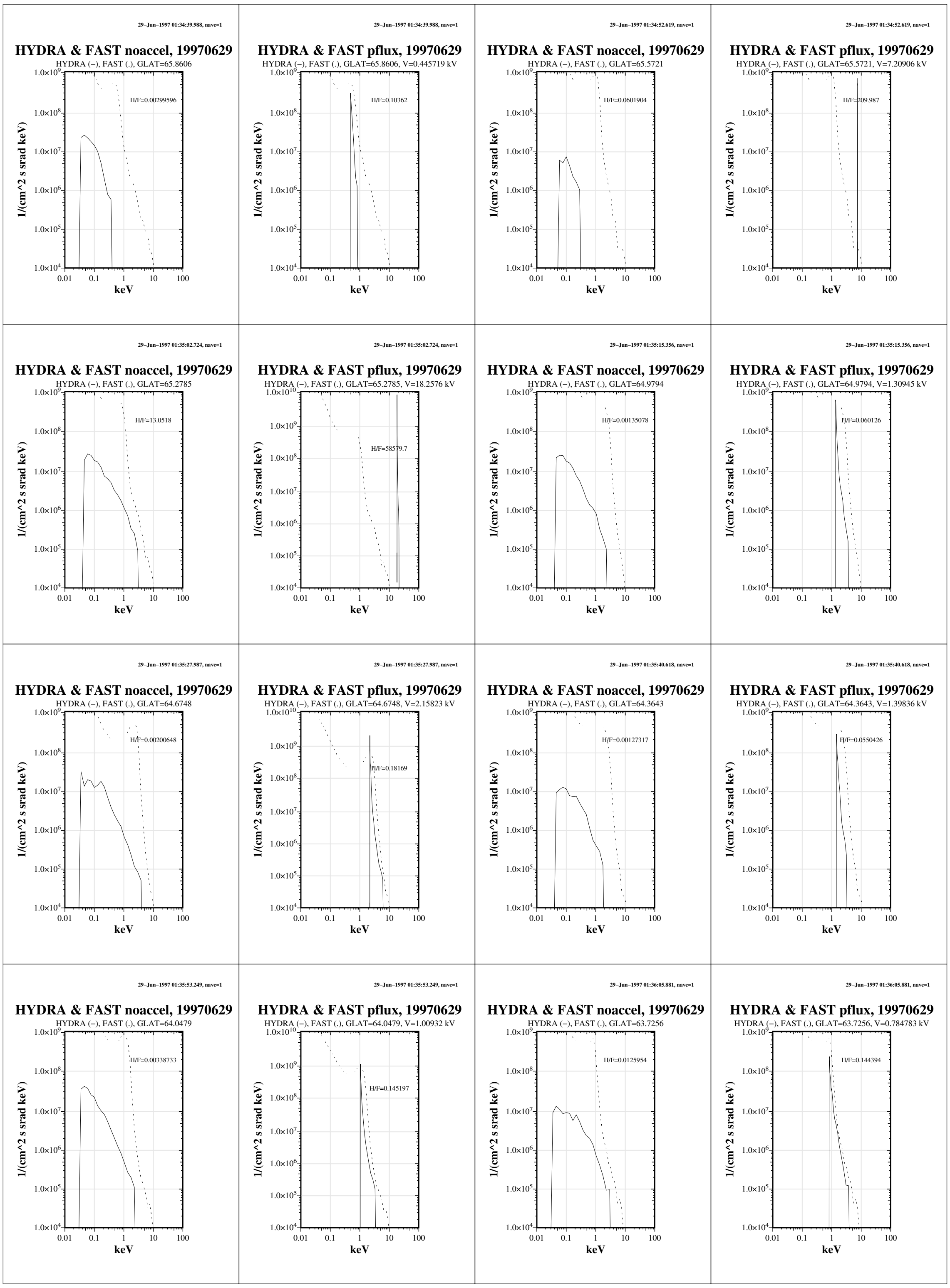

Figure 15: Same as Figure 15 but for 970629. No latitudinal shifting is done in this event.

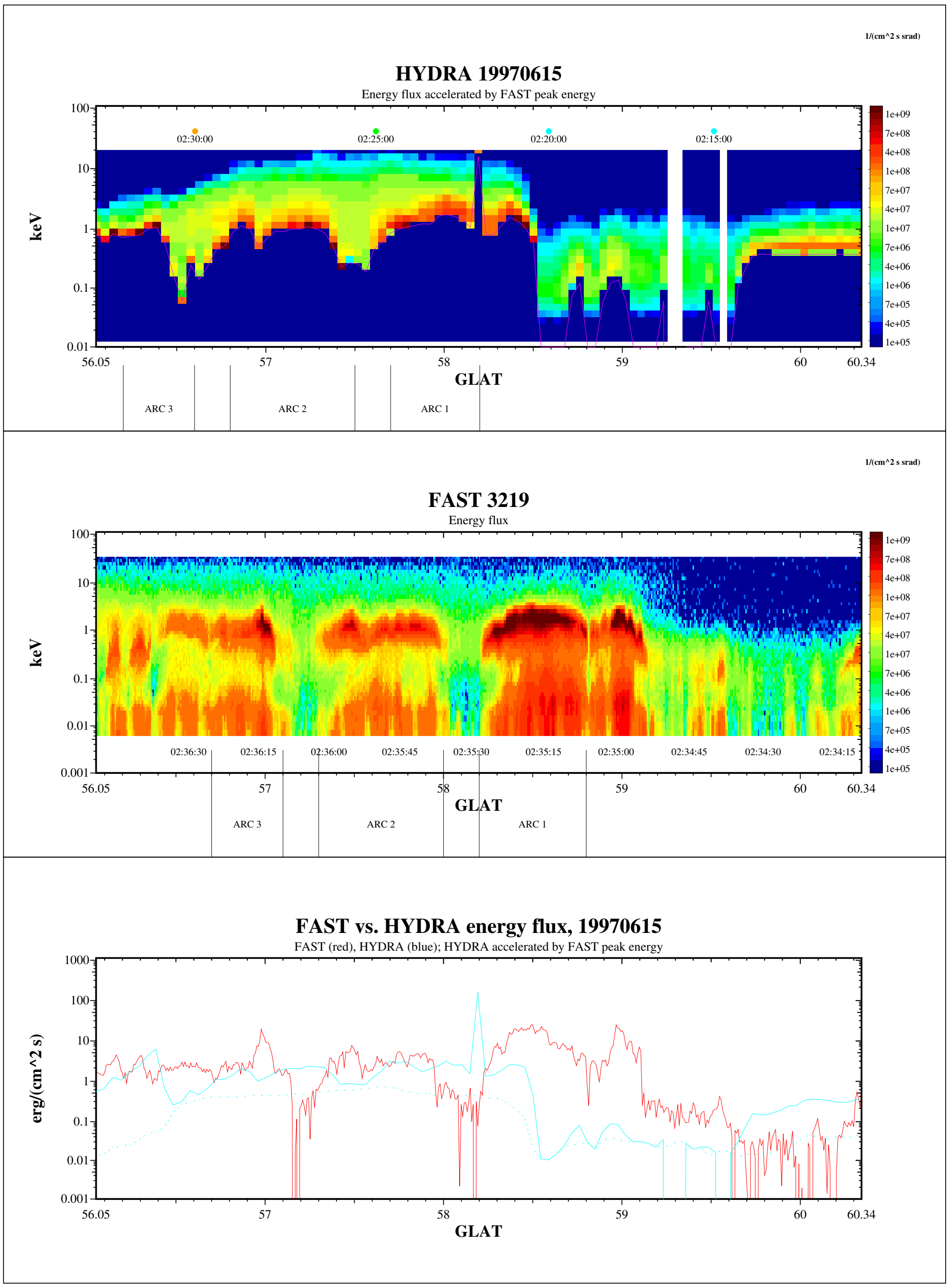

Figure 16: Upper panel: HYDRA electron energy flux accelerated by FAST peak energy. A latitudinal shift of 0.6 degree was included when finding the FAST peak energy. Middle panel: FAST energy flux. Lower panel: Comparison of FAST energy flux (red) with HYDRA accelerated energy flux (blue). The nonaccelerated HYDRA energy flux is also shown (dotted blue).

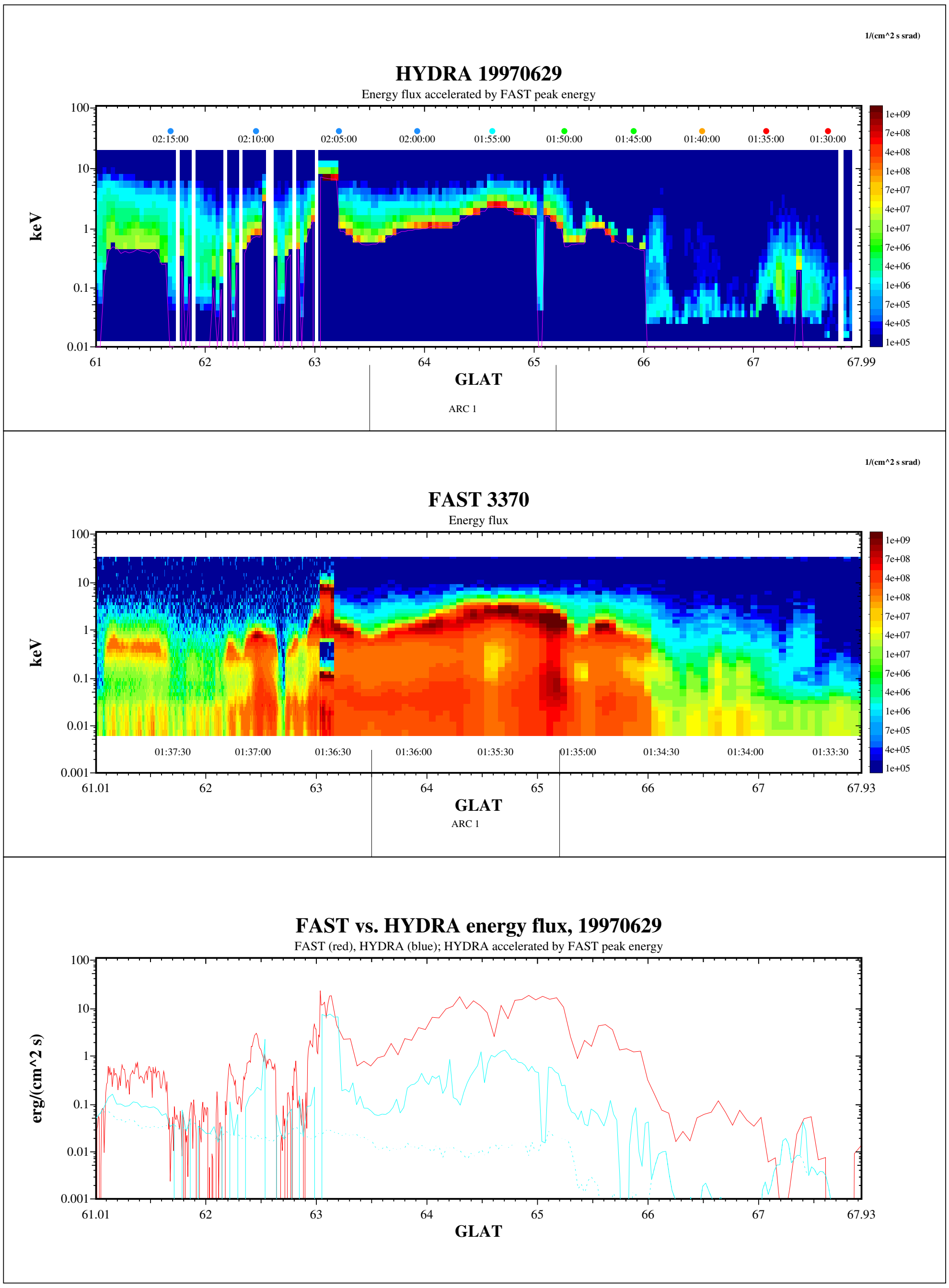

Figure 17: Same as Figure 16, but for 970629. No latitudinal shifting in this event.

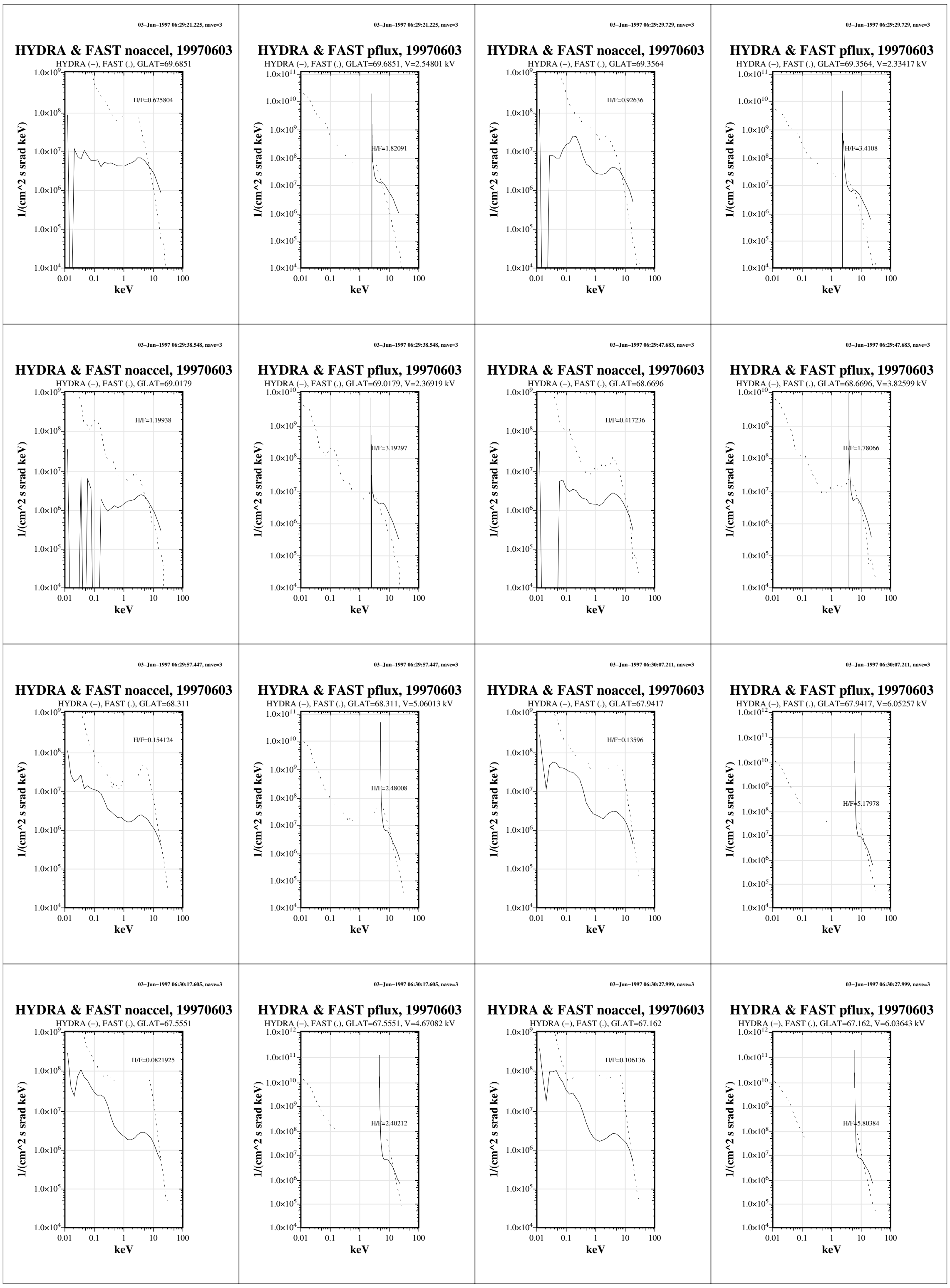

Figure 18: Same as Figure 14 but for 970603, where HYDRA data are of the multiple-Maxwellian type.

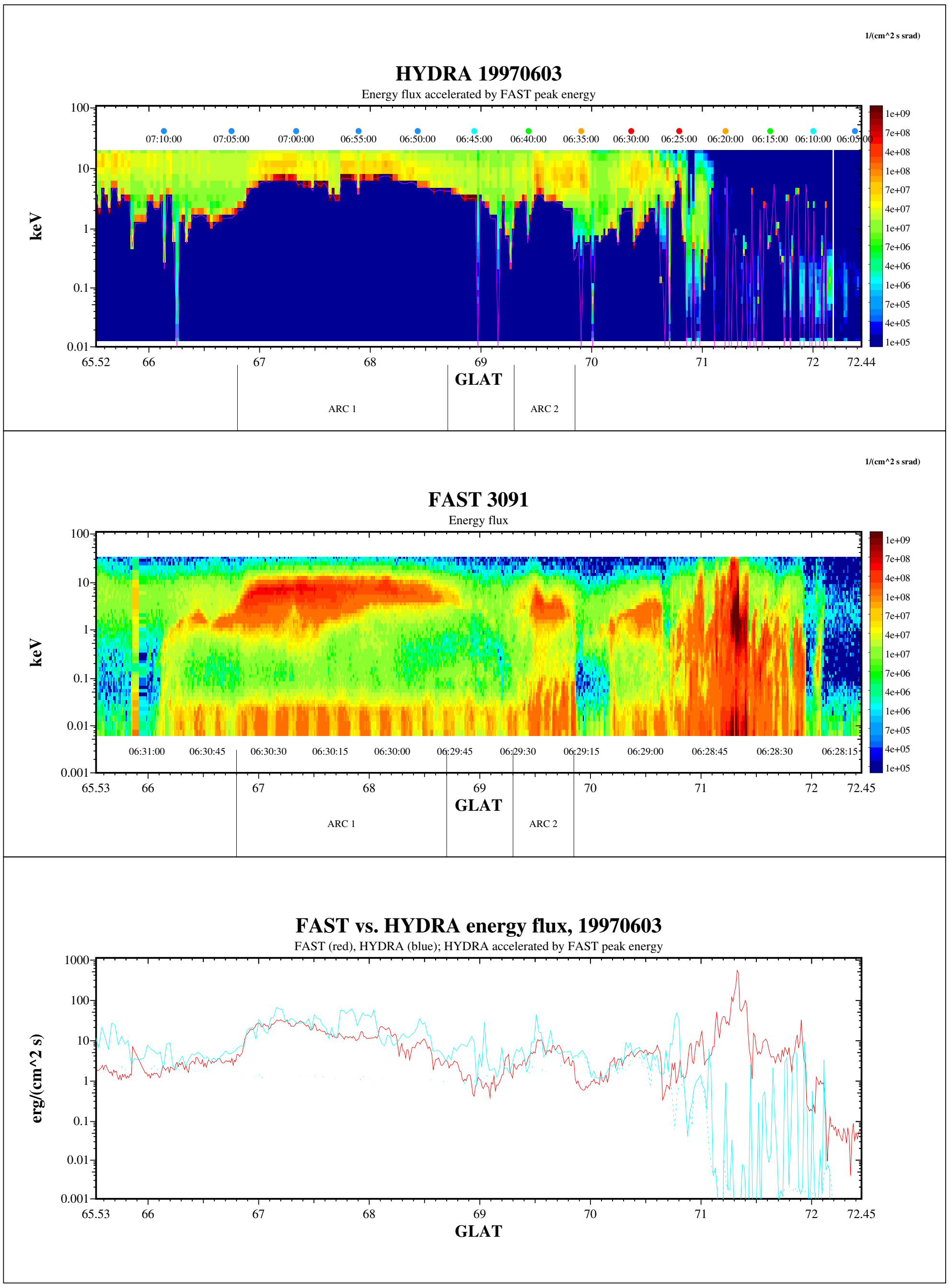

Figure 19: Same as Figure 16 but for 970603, where HYDRA data are of the multiple-Maxwellian type.

pretty well, but the matching of the functional form of the spectra is rather poor. The point is not only that the functional forms mismatch in these particular events, but also that the multiply-peaked HYDRA spectra produce very untypical-looking inverted-V spectra if accelerated through a potential drop. Thus questions such as mapping errors and temporal stability, which are always a concern in conjunction studies, do not affect this conclusion.

The fact that the integrated energy fluxes match after acceleration is not very surprising and should not be taken as an indication that the real energization process is necessarily a potential drop. Especially when the FAST potential V is clearly larger than the source plasma thermal energy T, variations in V cause corresponding variations in the accelerated energy flux, almost regardless of how the original HYDRA data look like. This is because the energy flux is under these conditions approximately proportional to $nT^{-1/2}V^2$ where n is the source plasma density [*Fridman and Lemaire,* 1980]. The energy flux is more sensitive to variations in V, which is determined by FAST data alone, than to variations in n or T, which are determined by HYDRA data.

The other multiple-Maxwellian events show a similar behavior as 970603.

4.3 Conclusions

One must note that the set of nine Polar/FAST conjunctions all happened during summertime, and most happened in June 1997. Thus the set of available conjunctions is not completely representative with respect to season. No clear correlations with Polar altitude can be seen in our nine events.

We conclude that

1. In diffuse precipitation events, FAST and HYDRA energy fluxes generally match rather well. FAST fluxes are typically about 2-3 times larger, however.

2. The diffuse events show that the mapping method is feasible and provide an independent consistency check for the correctness of the energy flux computation routines for the two spacecraft.

3. During inverted-V precipitation , FAST energy flux is typically 10 times higher than HYDRA energy flux.

4. Electrostatic wave activity and significant anisotropies are not present on a regular basis in single-Maxwellian events.

5. In one of the single-Maxwellian events (970615), matching of the spectra and the integrated energy flux is pretty good after acceleration by the FAST peak energy. In the other event (970629) the matching is not so good because the HYDRA population is too cold and somewhat deformed from a Maxwellian shape in this event.

6. Evidence for energized outflowing oxygen where the energy approximately matches the FAST peak energy was found in one of the two single-Maxwellian events (970629). The energy was 1-2 kV in this case.

7. The correspondence of the distribution functions between HYDRA and FAST in the multiple-Maxwellian events is complicated and cannot be explained by a U-shaped potential. The integrated energy fluxes can be made to match by assuming acceleration by a potential drop, but not the functional forms of the spectra.

8. TIMAS oxygen outflow in multiple-Maxwellian events was of the low-energy type when the situation was clear enough to allow determination, which speaks against a static potential drop.

9. In multiple-Maxwellian events there is a temporal correlation between short-lived (or spatially compact) electron anisotropy occurrences at middle (around 40-400 eV) energies, and broadband electrostatic wave bursts in the 4 Hz – 1 kHz frequency range (the 10-28 Hz range is not covered by the instruments however).

10. The single-Maxwellian events partly support and partly do not support the presence of a potential drop; the potential drop, if it exists, is small (1-2 kV) in any case. In the multiple-Maxwellian events, which show higher peak energies more typical of inverted-V events, a potential drop model of auroral energization leads to inconsistencies with the spectral shape and missing energization of upflowing oxygen, while it manages to reproduce the integrated energy flux magnitude rather well. We suggest that the energization is caused by some other mechanism in the multiple-Maxwellian events and that the observed occurrence and mutual correlation of the electron anisotropies and electrostatic wave bursts (see the previous Item) play a role in the acceleration process.

References

[*Carlqvist and Boström,* 1970] **Carlqvist, P. and R. Boström,** Space-charge regions above the aurora, *J. Geophys. Res., 75,* 7140–7146, 1970.

[*Carlson et al.,* 1998] **Carlson, C.W., R.F. Pfaff and J.G. Watzin,** The Fast auroral snapshot mission, *Geophys. Res. Lett., 25,* 2013–2016, 1998.

[*Evans,* 1974] **Evans, D.S.,** Precipitating electron fluxes formed by a magnetic field aligned potential difference, *J. Geophys. Res., 79,* 2853–2858, 1974.

[*Fridman and Lemaire,* 1980] **Fridman, M., and J. Lemaire,** Relationship between auroral electron fluxes and field aligned electric potential differences, *J. Geophys. Res. 85*, 664-670, 1980.

[*Gurnett et al.,* 1995] **Gurnett, D.A., A. M. Persoon, R. F. Randall, D. L. Odem, S. L. Remington, T. F. Averkamp, M. M. DeBower, G. B. Hospodarsky, R. L. Huff, D. L. Kirchner, M. A. Mitchell, B. T. Pham, J. R. Phillips, W. J. Schintler, P. Sheyko, and D. Tomash,** The Polar Plasma Wave Instrument, Space Sci. Rev., ed. by C. T. Russell, Kluwer Academic Publishers, 71, pp. 597-622, 1995.

[*Harvey et al.,* 1995] **Harvey, P., F.S. Mozer, D. Pankow, J. Wygant, N.C. Maynard, H. Singer, W. Sullivan, P.B. Anderson, R. Pfaff, T. Aggson, A. Pedersen, C.G. Falthammar and P. Tanskanen,** The electric field instrument on the polar satellite, Space Science Reviews 71, 583-596, 1995.

[*Janhunen et al.,* 1999] **Janhunen, P., A. Olsson, F.S. Mozer and H. Laakso,** How does the U-shaped potential close above the acceleration region? A study using Polar data, *Ann. Geophys., submitted,,* 1999.

[*Lin and Hoffman, 1979]* **Lin, C.S, and R.A. Hoffman,** Characteristics of the inverted-V event, *J. Geophys. Res., 84,* 1514-1525, 1979.

[*Moore et al.,* 1995] **Moore, T.E., C.R. Chappell, M.O. Chandler, S.A. Fields, C.J. Pollock, D.L. Reasoner, D.T. Young, J.L. Burch, N. Eaker, J.H. Waite, Jr., D.J. McComas, J.E. Nordholt, M.F. Thomsen, J.J. Berthelier and R. Robson,** The Thermal

Ion Dynamics Experiment and Plasma Source Instrument, Space Sci. Revs., 71, 409, 1995.

[*Mozer et al.,* 1977] **Mozer, F.S., C.W. Carlson, M.K. Hudson, R.B. Torbert, B. Parady, I. Yatteau and M.C. Kelley,** Observations of paired electrostatic shocks in the polar magnetosphere, *Phys. Rev. Lett.,* 38, 292, 1977.

[*Reiff et al.,* 1988] **Reiff, P.H., H.L. Collin, J.D. Craven, J.L. Burch, J.D. Winningham, E.G. Shelley, L.A. Frank and M.A. Friedman,** Determination of auroral electrostatic potentials using high- and low-altitude particle distributions, *J. Geophys. Res., 93,* 7441–7465, 1988.

[*Shelley and Collin,* 1991] **Shelley, E.G. and H.L. Collin,** Auroral ion acceleration and its relationship to ion composition, in Auroral physics, Meng, Rycroft and Frank (eds.), Cambridge University Press, 1991.

[*Shelley et al.,* 1995] **Shelley, E.G., A.G. Ghielmetti, H. Balsiger, R.K. Black, J.A. Bowles, R.P. Bowman, O. Bratschi, J.L. Burch, C.W. Carlson, A.J. Coker, J.F. Drake, J. Fischer, J. Geiss, A. Johnstone, D.L. Kloza, O.W. Lennartsson, A.L. Magoncelli, G. Paschmann, W.K. Peterson, H. Rosenbauer, T.C. Sanders, M. Steinacher, D.M. Walton, B.A. Whalen and D.T. Young,** The Toroidal Imaging Mass-Angle Spectrograph (TIMAS) for the Polar Mission, Space Science Rev., 71, 1-4, 1995.